Knock recognition based on vibration signal and Wiebe function in a heavy-duty spark ignited engine fueled with Methane

Pierpaolo Napolitano[b], Irina Jimenez[a], Benjamín Pla[a], Carlo Beatrice[b]

[a] *CMT-Motores Termicos, Universitat Politecnica de Valencia, Camino de Vera s/n, E-46022 Valencia, Spain.*
[b] *Consiglio Nazionale delle Ricerche, Piazzale Aldo Moro,7, Rome RM, Italy.*

Abstract

Increasing demands on higher performance and lower fuel consumption and emissions have lead the path for internal combustion engine development; this race is nowadays directly related of CO2 emissions reduction. In spark-ignited (SI) engines, knock is one of the major barriers to achieve high thermal efficiency at high loads. The knocking risk is even higher in heavy-duty (HD) engines due to the size of the cylinders and to the low rotation speed. This paper proposes a knock detection strategy based on the combination of knock sensors and combustion modeling applied to a HD natural gas (NG) engine. The aim is to have a reliable, economic and computationally efficient algorithm to be implemented directly on the engine ECU.

The method proposed has been applied to an extensive set of experimental data acquired on a SI NG heavy-duty engine. The results of the proposed knock estimation method are benchmarkt with those based on in-cylinder pressure analysis using piezoelectric transducers. The extension of the method based on in-cylinder pressure to a high displacement heavy-duty NG engine not only represents an innovation, but improves the knock recognition based on in-cylinder pressure compared with conventional methods as MAPO or IMAP. Besides, the development of an alternative method based on knock sensor signal, allows to obtain a higher or equal sensitivity compared to the traditional MAPO method based on in-cylinder pressure, with the advantage of only using knock sensors.

Keywords: knock, heavy-duty engine, resonance, wiebe function

1. Introduction

In recent years, diverse legislative measures have been implemented by international regulatory agencies in order to increase the development of alternative fuels in transport systems [1]. One of the most widely investigated alternative fuels found in literature is Natural Gas (NG) [2], which is a gas mixture consisting primary of methane, with smaller percentages of other gases such as ethane, propane, and butane.

The recent sensibility in the reduction of CO2 emissions from thermal system has pushed the research to the use of alternative low carbon content fuels, and they diffusion to any possible combustion system [3]. The sector of heavy duty (HD) engine for road and off-road application was not excluded from this phenomena [4]. Since NG has a higher octane number than gasoline, it is possible to work with higher compression ratio in spark ignition (SI) engines [5, 6]. Nevertheless, using a gas instead of a liquid fuel involves the displacement of some air by NG, then leading to a reduction in the engine power output in port fuel injection cases [7]. In order to overcome this problem, two solutions can be found in literature: on the one hand, increasing the compression ratio, or in the other hand using lean combustion [8, 9]. However, the compression ratio increase is limited by knock phenomena in SI engines due to higher combustion pressures and temperatures [9, 6], and as regards lean combustion, this has an operation limit, i.e over lean the mixture may lead to instability and misfire [10, 11].

Knock is an abnormal combustion phenomena in SI engines, related with the uncontrolled combustion of the end gas [12]. When knock occurs, a rapid combustion is observed due to the high local pressure, which produces shock waves that heavily excite the in-cylinder resonant modes [13, 14]. The engine exposition to knock during several cycles may lead to piston rings braking, piston melting, engine efficiency decrease and engine damage in general [15].

On this way, knock recognition techniques are important in order to achieve high thermal efficiency. These methods can be mainly classified in two principal groups: direct and indirect knock recognition methods [15]. The first group is based on the in-cylinder pressure measurement, which is directly influenced by the phenomena [13,

16, 17]. The second group is based on indirect measurements such as cylinder block vibration [18, 19]. Despite methods based on in-cylinder pressure measurement show higher reliability and accuracy, their application in mass production engines is limited by sensors durability and cost [20, 21].

Classical knock recognition techniques are based on a fixed threshold, as the Maximum Amplitude of Pressure Oscillations (MAPO), which consist on comparing the absolute value of the band-pass filtered pressure signal with a predefined threshold [22]. Some authors developed knock metrics for knocking recognition [23, 24], or classification models as is shown in [25], where a machine learning algorithm is presented. Recently, knock recognition methods had been developed with the aim of being able to recognize knocking events from combustion without the need of a fixed threshold. For example, in [17] the band-pass in-cylinder pressure is compared in two windows locations: at the main combustion process location and at the end of combustion. The comparison between the signal amplitudes at both locations allows to identify low intensity knocking cycles. Additionally, a knocking threshold based on Mass Fraction Burned (MFB) evolution is presented in [13], where knocking cycles are differentiated from normal combustion using a resonance index which is compared with the expected resonance index produced by a constant volume combustion of the remaining fuel. Although these methods show good results and are able to recognize knock, even with low intensity, they are in-cylinder pressure based, which makes its application expensive in production engines [26].

Regarding knock recognition methods based on vibration signal, in recent years several indexes based on Fast Fourier Transform (FFT) [27], Empirical Mode Decomposition (EMD) [28] or Walvelet [18] analysis have been developed. The main problem with these approaches is the need to set a threshold in order to distinguish knock from normal combustion.

The objective of the present work is to develop an improved understanding of the information contained in the knock sensor signal by analyzing two different sensor locations. The novelty of this work is to extended the method presented in [13] for a light-duty SI engine based on in-cylinder pressure signal, to a heavy-duty SI engine basing the method on knock sensor signals.

This work is organized as follows, first the experimental set-up and tests performed are presented. Then, a frequency analysis of both knock sensor signal positions is performed and compared with in-cylinder pressure signal information. After, the knock recognition method is presented, where the MFB model and the knock recognition procedure are introduced. Then, results and discussions about the MFB model and the knock recognition are presented. The final section highlights the main contribution of the work and proposes future work for control applications.

2. Experimental set-up and tests

Experimental tests for calibration, illustration and validation proposes were carried out in a heavy-duty NG SI engine. The engine was coupled with a variable frequency fast response dynamometer (AVL Dynodur), able to perform tests both in steady state than in transient conditions. The engine was full instrumented and monitored, all low acquisition frequency measures were made by a National Instruments DAQ device. Instead, high sampling rate indicated signals were acquired and recorded by means of an AVL IndiSmart indicating system coupled with the AVL Indicom software. The main specifications of the engine are collected in Table 1.

Table 1: Engine main specifications

Displaced volume	5883 cc
Stroke	120 mm
Bore	102 mm
Compression ratio	10.3:1
Number of cylinders	6
Valves per cylinder	2
Injection system	Multy point. Port Fuel Injection (PFI)
Fuel	Methane
Rated power	117kW
Max torque	630Nm

In order to analyze the information contained in the knock sensor signal and evaluate the knock recognition method, two cylinders were equipped with in-cylinder pressure sensors (cylinders 1 and 3) as is indicated in Figure 1. The in-cylinder pressure sensor used are two measuring spark plug with miniature piezo-electric pressure transducer from Kistler, type 611xC. In addition, signals from three knock sensors, piezo-quartz accelerometer with integrated discharge resistor (4.8 M Ω), with a nominal sensitivity of 30 mV/g, max mechanical vibrations 70 g_{peak}, were installed in different positions of the engine block were analyzed: two of them in correspondence with the cylinders 1 and 3 location (Ks A and B) and a third located between both cylinders (Ks C).

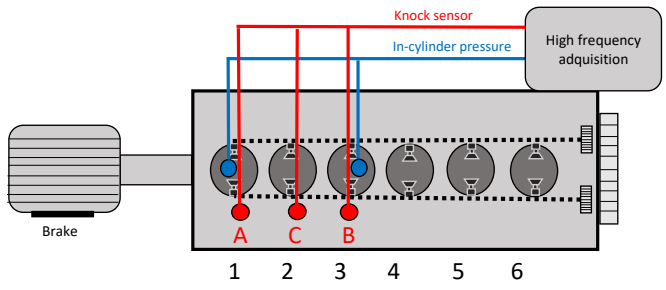

Figure 1: In-cylinder and knock sensors configuration.

Knock sensors A and B correspond to a case where six sensors are required for knock recognition, i.e. one for each cylinder. On the other hand, knock sensor C represents the case where two knock sensors are necessary to evaluate knock in all six cylinders, one near cylinder 2 as is shown in Figure 1 and a second one near cylinder 5.

The sampling frequency for knock and pressure sensors was of 0.05 CAD. During the experiments, the engine was tested at different steady operating conditions by keeping the speed and load constant while the Spark Advance (SA) was modified. For every testing point, the SA was progressively advanced from the reference value with 2 CAD steps until a maximum advance of 6 CAD. The operating conditions in terms of speed and load are represented in Figure 2, where the conditions used for model calibration and validation can be identified. For the analysis of the data the instantaneous engine speed fluctuations during tests are negligible.

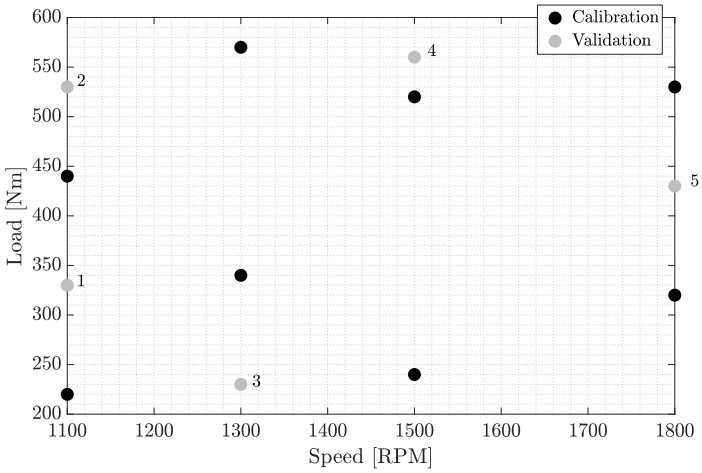

Figure 2: Calibration and validation tests performed.

3. Frequency analysis of knock sensors signals

During this section, the frequency content of signals from knock sensors A and B will be compared with the signal from knock sensor C. For this, each knock sensor signal is compared with the correspondent in-cylinder pressure signal, i.e. cylinder 1 with A and C, and cylinder 3 with B and C.

In order to estimate the resonance frequencies during knocking and no-knocking cycles, the approach presented by Draper [29] is used. In [29], the wave equation was solved with Bessel functions for a cylindrical geometry, showing that the characteristic frequency generated in the combustion chamber can be expressed as:

$$f_{(i,j)} = a_s \sqrt{(\frac{B_{(i,j)}}{\pi D})^2 + (\frac{g}{2h})^2} \quad (1)$$

where the axial modes g are neglected near the TDC because the height is too low ($h <$ D), D is the bore of the cylinder, a_s the speed of sound and $B_{(i,j)}$ are the Bessel constants related with the radial modes, i and j represent the number of circumferential pressure modes and number of radial pressure modes. The speed of sound can be calculated by measuring the trapped mass m, the in-cylinder pressure p, and estimating the instantaneous volume of the chamber V.

$$a_s = \sqrt{\frac{\gamma p V}{m}} \quad (2)$$

where γ is the specific heat capacities ratio of the gases inside the cylinder, which can be approximated by dividing the gas mixture in three species, namely air, fuel, and burnt products, and modeled by polynomial expressions for the in-cylinder temperature such as suggested in [30].

The spectrogram of each in-cylinder pressure signal (P1 and P3) and knock sensors signals (A, B and C) are shown in Figures 3 and 4. In Figure 3, cylinder 1 is a knocking cycle while cylinder 3 a normal combustion cycle, and in the Figure 4 it is the opposite case, i.e. cylinder 1 normal combustion cycle and cylinder 3 knocking cycle. In dashed white line, the resonance frequency computed from Equation (1) is represented for the first 3 radial modes. The operating conditions of such spectrograms is 1500 rpm of engine speed and 525 Nm of load.

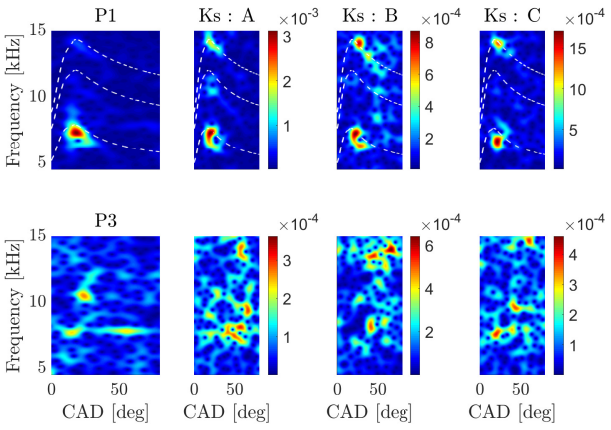

Figure 3: Spectogram of in-cylinder pressure signals (left), and knock sensors A, B and C. Cylinder 1 is knocking cycle and cylinder 3 a normal combustion cycle. Cycle 120 of the data set.

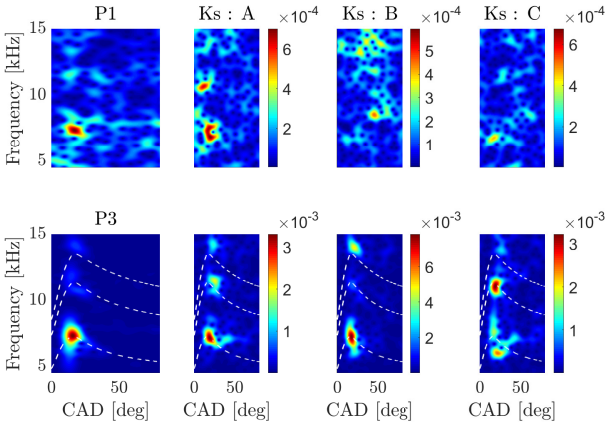

Figure 4: Spectogram of in-cylinder pressure signals (left), and knock sensors A, B and C. Cylinder 3 is knocking cycle and cylinder 1 a normal combustion cycle. Cycle 78 of the data set.

Analyzing Figures 3 and 4, the resonance components in the in-cylinders pressure signals are also present in the three knock sensor signals. For the cases where the knock sensor is located near the cylinder, knock sensor A for cylinder 1 and knock sensor B for cylinder 3, the intensity of the resonance components are higher comparing with the others knock sensors (as can be seen in the color bar of each plot). It is noticeable that as the distance from the knock sensor increases, the intensity of the resonance decreases. Notice that the different peaks present in knock sensor A, B or C corresponds to the different resonance frequencies computed from Equation (1), as an example 3 resonance modes were represented.

In order to assess several cycles, the correlation between the information contained in knock sensors signals and the in-cylinder pressure signals is analyzed by computing the coherence function between them. The coherence functions is the the ratio between the cross power spectral density of the in-cylinder pressure (sub-index p) and knock sensor (sub-index k) signals $P_{p,k}(f)$, to the product of the power spectral density of each signal $P_{p,p}(f)$ and $P_{k,k}(f)$. This relation is computed as [31]:

$$C_{p,k}(f) = \frac{|P_{p,k}(f)|^2}{P_{p,p}(f)P_{k,k}(f)} \tag{3}$$

where f represents the different frequencies and the power spectral density of a signal x is defined as:

$$P_{x,x}(f) = \sum_{k=-\infty}^{k=\infty} r_{xx}[k]e^{-i2\pi fk} \tag{4}$$

where r_{xx} is the auto correlation function, which is computed as a sliding inner product of the signal x with itself::

$$r_{xx}[k] = x[n]x[n+k] \tag{5}$$

And the cross power spectral density between two signals x and y is defined as follows:

$$P_{p,k}(f) = \sum_{k=-\infty}^{k=\infty} r_{xy}[k]e^{-i2\pi fk} \tag{6}$$

where r_{xy} is the cross correlation function, which is computed as:

$$r_{xy}[k] = x[n]y[n+k] \tag{7}$$

The coherence function between the in-cylinder pressure and knock sensor signals ($C_{p,k}$) was evaluated at high load steady operating condition, 1300 rpm 570 Nm, over 200 cycles in Figure 5, where knocking and no-knocking cycles were part of the data-set. The black line line represents the evolution of the coherence function for knock sensor A while purple and blue show the results for knock sensors B and C respectively. The left plot shows the results for cylinder 1, while the results for the cylinder 3 appear in the right plot. Three frequencies has been highlighted in red line, these frequencies corresponds to the maximums of the first three resonance modes for this operation condition. Also notice that the x-axis scale of both plots it is logarithmic.

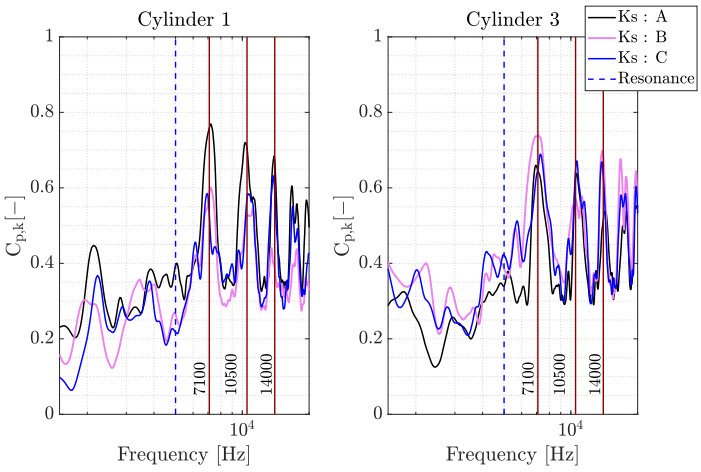

Figure 5: Coherence function between in-cylinder pressure and knock sensor signals. Cylinder 1 (left) and Cylinder 3 (right).

As can be seen in Figure 5, the coherence with the in-cylinder pressure signal computed from cylinder 1 is lower for knock sensor B than for knock sensors A or C. Analogously, for cylinder 3 case, the lowest coherence corresponds to knock sensor A while sensor B shows the highest coherence in the high frequency region. In both cases, the coherence is related with the distance between cylinder and knock sensor location. Notice that at the three frequencies highlighted in red the coherence function reach the maximum value. From these three comparisons, it can be seen that the mean coherence between the in-cylinder pressure and knock sensor is high, over 0.5, but in specific frequency bands, which are related with the in-cylinder resonance frequency modes computed from Equation (1).

The analysis of high frequencies components of in-cylinder pressure signals and knock sensor signals was performed by computing an alternative of the Fourier transform as is described in [32]. Here, a resonance index is computed from in-cylinder pressure signal as following:

$$I_p(\alpha) = \sum_{\alpha=\alpha_1}^{\alpha=\alpha_2} w(\alpha-\alpha_1) p_{bp}(\alpha) e^{-2\pi \sum_{\psi=0}^{\psi=\alpha} \frac{B_{i,j}\sqrt{\gamma(\psi) p_{lp}(\psi) V(\psi)}}{\pi D \sqrt{m}}} T_s(\alpha) \tag{8}$$

where α_1 and α_2 define the interval where the resonance analysis is performed, w is a window function of $\alpha_2 - \alpha_1$ length, p_{bp} the band-pass filtered pressure, and $T_s(\alpha)$ is the sampling period, which is constant only in time-based acquisition or if the instantaneous engine speed fluctuations are negligible, $B_{i,j}$ is the Bessel constant [29], D is the bore of the cylinder, V the combustion chamber volume, m the trapped mass, and p_{lp} the low-pass in-cylinder pressure.

Analogously to the Equation (8), a resonance index can be defined from the knock sensor signals, as:

$$I_k(\alpha) = \sum_{\alpha=\alpha_1}^{\alpha=\alpha_2} w(\alpha-\alpha_1) ks_{bp}(\alpha) e^{-2\pi \sum_{\psi=0}^{\psi=\alpha} \frac{B\sqrt{\gamma(\psi) ks_{lp}(\psi) V(\psi)}}{\pi D \sqrt{m}}} T_s(\alpha) \tag{9}$$

where ks_{bp} and ks_{lp} are the band and low pass knock sensor signals respectively.

In Figure 6, the resonance index is compared with the band-pass signal, filtered between 4.5 and 15 kHz. In black line the resonance index evolution is shown and in grey line the band pass signal. Three different signals are analyzed during the same cycle: on the top, in-cylinder pressure from cylinder 1, on the middle, the knock sensor A, and on the bottom, knock sensor C.

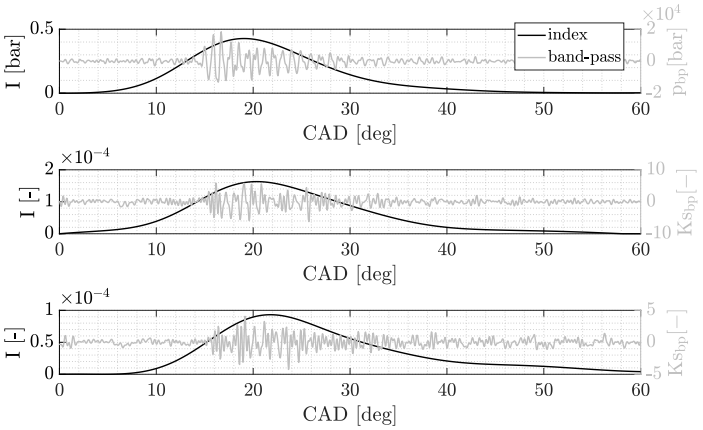

Figure 6: Resonance index evolution for cylinder 1 resonance evaluation: In-cylinder pressure (top), knock sensor A(middle) and C (bottom).

Analyzing Figure 6 the resonance index from the three signals during this specific cycle evolves in a similar way. However, the in-cylinder pressure index maximum is located earlier than both knock indexes. When comparing knock sensor A with C index, the maximum corresponding to knock sensor A is located earlier than C, this could be due to the fact that the knock sensor A it is located closer to the cylinder 1. On the other hand, the maximum amplitude computed from knock sensor A is higher than knock sensor C.

In order to evaluate resonance in several cycles, from the resonance index two parameters had been extracted: the amplitude of the maximum, which is directly related with the amplitude of the resonance oscillation, and the location of such oscillation, i.e the location of the maximum of the resonance index. Following, the results from knock sensors signals and the in-cylinder pressure signal had been compared in Figure 7. On the left plot, the maximum amplitude from in-cylinder pressure is represented against the

maximum from knock sensors signals. On the right plot, the error between the location of such maximum is shown. Different colors are used to differentiate the knock sensors signals, black color is used to represent data obtained from knock sensor A, and grey color from knock sensor C. In black the R^2 value of all data is shown and in blue the R^2 value of the relative region (over 0.5 bar of resonance amplitude was considered).

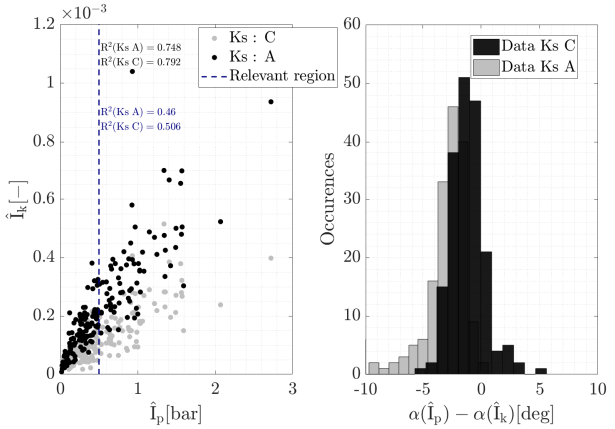

Figure 7: Resonance index parameters obtained from in-cylinder pressure compared to knock sensors A and C. Left plot: Maximum amplitude of the indicator. Right plot: error histogram of the maximum location of the indicator.

As can be seen in Figure 7 (left), the maximum amplitude of the index for knock sensor A is higher than for case knock sensor C, this is due to the fact that the knock sensor A is located closer to cylinder 1. For the location parameter (right plot), the correlation between the observation from knock sensors and in-cylinder pressure is slightly affected by the location of the sensors, and for the case of knock sensor A the error is lower than for knock sensor C. For the case of the maximum amplitude, left plot, the R^2 value for both cases is over 0.7, which can be considered a strong effect size, while for the R^2 value in the relevant region is considerable lower in both cases. But for the location case, right plot, the knock sensor position has more effect on this parameter, since low amplitude cases leads to have more deviation from the measurement from in-cylinder pressure. Despite the lower R^2 value for the relevant zone (high amplitudes of resonance), in later section during the calibration process of the knock recognition method this point will be addressed.

As it was shown in [13], the maximum amplitude and location of the resonance index computed from in-cylinder pressure signal it is highly sensitive to the SA. In cycles without knock, maximum amplitudes tend to be moderate and located in the surroundings of the center of combustion (MFB_{50}). On on the other hand, in knocking conditions the amplitude increases and the location of the maximum happens to be located after the MFB_{50}, closer to the end of combustion.

Figure 8 shows the distribution of the resonance index for cylinder 1 using knock sensor A (top plots) and C (lower plots). The number of occurrences in terms of the maximum location respect to the MFB_{50} and the amplitude are shown for 3 SA cases: left cases the SA is set at the reference value (SA_{mv}), middle and right cases show results advancing the SA 2,5 and 5,5 CAD respectively.

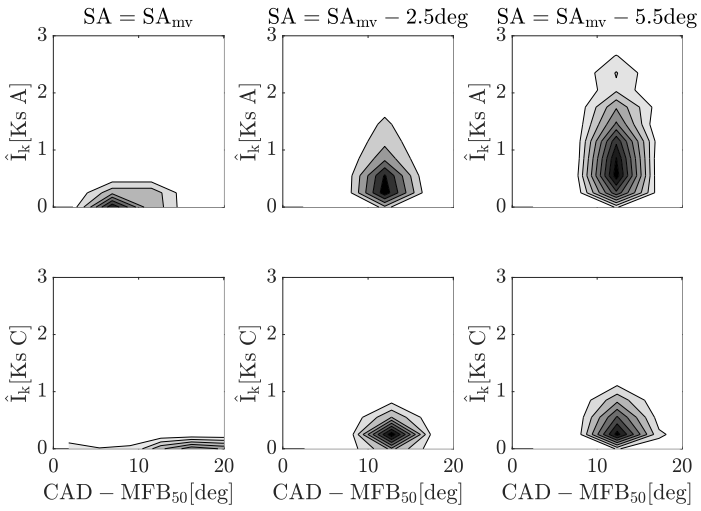

Figure 8: Number of occurrences in terms of maximum location and amplitude resonance index respect to cylinder 1. Top plots Ks A and bottom plot Ks C.

Analyzing Figure 7, the resonance index computed from knock sensor A is more sensible to the SA change than knock sensor C, pointing out that, as expected, knock is easily identified if a sensor is placed near the cylinder. However, results with knock sensor C, still show potential for knock detection.

4. Knock recognition method

The knock recognition method presented in [13] is used to develop a recognition technique based on knock sensor signal. The knock recognition method is proposed in this work is shown in Figure 9.

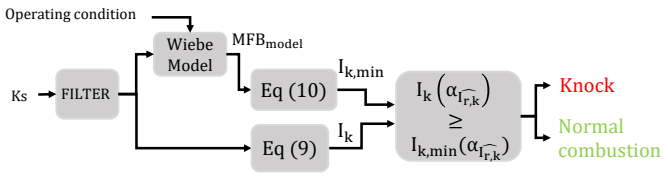

Figure 9: Scheme of knock recognition method based in knock sensor signal.

The knock classification is performed by comparing the resonance index, I_k, obtained from Equation (9), with the minimum oscillation resulting from the end gas to auto ignited, $I_{k,min}$, which is estimated as:

$$I_{k-min} = G_k P_{eg} \tag{10}$$

where P_{eg} is the pressure increase due to constant volume combustion of the end gas, and G_k represents a gain from pressure increase to amplitude of the resonance indexes, which might be calibrated.

The pressure increase due to constant volume combustion of the end gas can be written using the first law of thermodynamics as:

$$P_{eg} = \frac{\kappa - 1}{V} m_f H_p (1 - MFB_{model}) \tag{11}$$

where H_p the low calorific value of the fuel, m_f the fuel mass injected and MFB_{model} the MFB from the combustion model, and κ is the adiabatic exponent and V is the cylinder volume.

For this application, the minimum oscillation presented in Equation (10) instead of using the MFB computed from in-cylinder pressure signal as described in [13], the MFB is estimated from a pre-calibrated Wiebe function, which strongly simplifies the calculations and contributes to a future ECU implementation. After, following the scheme on Figure 9, the knock recognition is performed by comparing the amplitude of the maximum resonance index, with the value of the minimum oscillation evaluated at the crank angle position of the maximum resonance index, $I_{k,min}(\alpha_{\hat{I}_k})$. The comparison of the amplitude is performed in the crank angle position where the maximum resonance is reached because, not only the intensity of the resonance, but also the location with respect to the center of combustion characterize the cycles with knock or normal combustion (see Figure 8).

4.1. Calibration process

In this section, the calibration process of the transference constant G_k in Equation 10 is explained.

The calibration was performed from the in-cylinder pressure measurements, where the difference between the resonance indicator I_p and I_{p-min} was computed and compared against the difference between the measurement from knock sensor signal and combustion model, i.e. I_k and I_{k-min}. These differences are represented in Figure 10, where the red dashed line represents the knock on-set detected by the method when in-cylinder pressure is used.

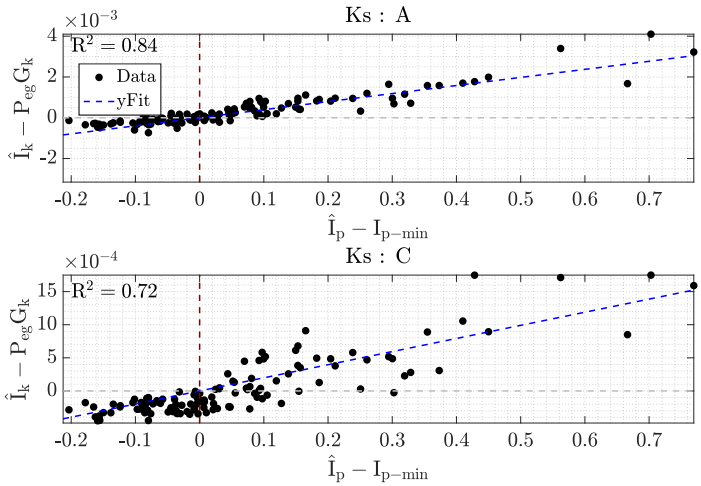

Figure 10: Data from calibration process: Knock sensor A (top) and knock sensor C (bottom).

Notice that the linear regression used $yFit$ has to be zero when $I_p - I_{p-min} = 0$, as this is the division between knocking and no-knocking cycles. Here, and even though the R^2 value in Figure 7, it can be notice that the R^2 related to knock evaluation is higher.

The calibration of G_k was performed by minimizing the distance of the data from the fitted line $yFit$, i.e $min|yFit - P_{eg}G_k|$. This calibration process was performed for knock sensors A, B and C separately over the calibration points detailed in Figure 2.

4.2. Mass fraction burned Wiebe model

In order to simplify the estimation of the MFB a pre calibrated Wiebe function is used, where the parameters $\dot{x}$ of the function are obtained from an Open Loop (OL) map as in terms of the operating condition (speed and load). In this work, the End Of Combustion (EOC) is estimated from knock sensor signal and the Start Of Combustion (SOC) is assumed to be in the SA.

The model used to estimate the MFB is represented in Figure 11, where x represents the Wiebe function constants, and α the crank angle.

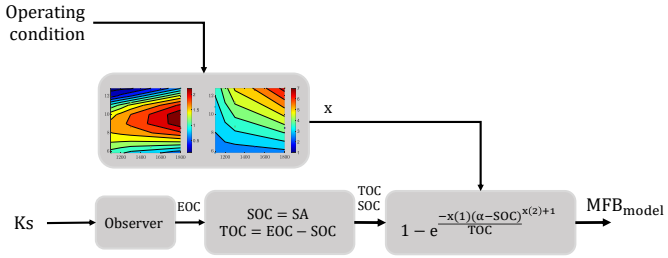

Figure 11: MFB wiebe model proposed.

The MFB wiebe model was calibrated over the calibration operating conditions shown in Figure 2. In order to compensate the model bias when it is applied to operating conditions different from those used for calibration, an observer of the combustion duration is introduced.

4.2.1. Observer

From the knock sensor signals the EOC is estimated as presented in [33], where the signal is denoised with a low-pass filter in order to remove high frequencies. An example is shown in Figure 12, where the denoise knock sensor signal is shown. In [33], the end of combustion is correlated with the fourth maximum, starting from the first peak.

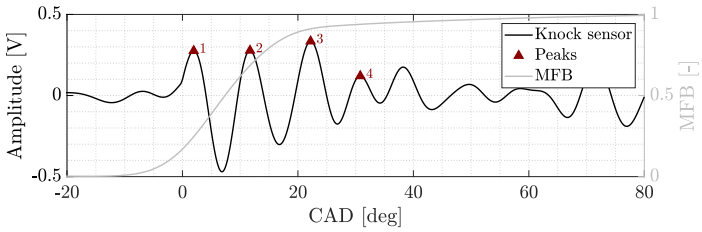

Figure 12: EOC observer from knock sensor signal.

The low-pass filtered knock sensor signal from A and C is represented in Figure 13, where in blue the mean MFB of the data-set is represented and in dashed red line the average angle of the CA90 is also highlighted.

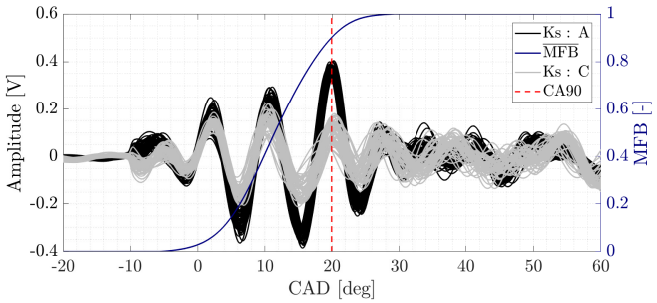

Figure 13: EOC observer from knock sensor signal.

As can be seen in Figure 13, low-pass signal from knock sensor A is less noisy than for the case of knock sensor C. Besides, the amplitude of the 4th peak is lower for knock sensor C.

The EOC was estimated from the vibration signal for 4 different speeds, results are shown in Figure 14. On the left, the EOC estimated from vibration signal A is compared with the CA90 computed from in-cylinder pressure 1. On the left, the rsquared over the 4 engine speeds are shown when computing the EOC from knock sensor A, filled points, and C, empty points. Different colors are used to differentiate the operating condition.

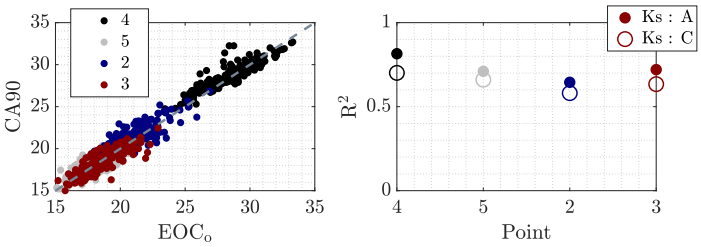

Figure 14: Pressure peak location against the CA90 for 4 operating conditions cylinder 1.

Notice in Figure 14 (left) that the CA90 obtained from the MFB computed from in-cylinder pressure sensor fit with the value obtained from the knock sensor estimation, this can be observed in the right plot, where for all four operating points the R^2 value is over 0.65 for knock sensor A and over 0.55 for knock sensor C.

Since the vibration signal is susceptible to noise, it is suggested to estimate the TOC by using an infinite input response (IIR) filter, as follows:

$$TOC^k = TOC^k(1 - \alpha_f) + TOC^{k-1}\alpha_f \qquad (12)$$

where k is the cycle, and α_f a value between 0 and 1, must be chosen to ensure a fast adaptation in transient operating conditions. In the present work a value of 0.9 has been selected.

5. Results and discussion

During this section results from MFB model and knock recognition method applied to the different knock sensors signals are analyzed. First, the results from the MFB model are compared with the measurements from in-cylinder pressure. Then, the knock recognition method is applied to cylinders 1 and 3, by running the method for both knock sensors location for each case.

5.1. Mass fraction burned model

As already introduced above, the MFB was estimated by estimating the EOC thought the knock sensors signals and by assuming the SOC to be at the SA. With these parameters, a Wiebe function is used to estimate the MFB evolution during a cycle.

In order to evaluate the error of the MFB estimation when using knock sensor A, B or C for EOC computation, three MFBx where computed, that is CA10, CA50 and CA90. In Figure 15 the absolute error between the estimation of such parameters and the value obtained from the in-cylinder pressure are shown for two cases: top plots when computing EOC from knock sensor A and B, and bottom plots when computing EOC with knock sensor C over validation point 4. Different colors are used to represent the different cylinders, grey color is used for cylinder 1 and blue for cylinder 3.

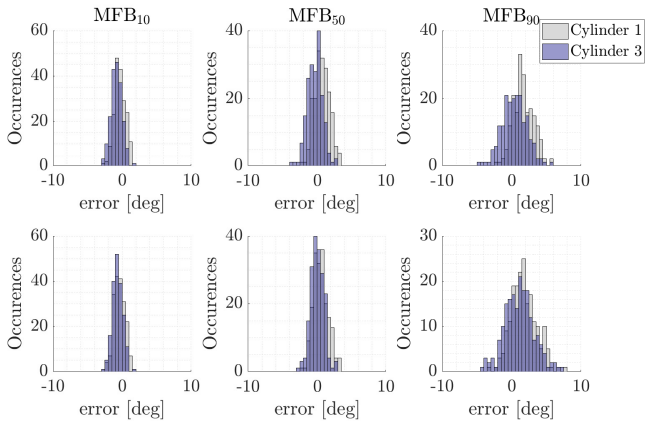

Figure 15: Error histograms between MFBx obtained from in-cylinder pressure and MFB model. Top plots knock sensors A and B, bottom plots knock sensor C. Operating condition point 4.

The estimation of the MFBx was performed over the validation data set points shown in Figure 2 (points 1 to 5). The error is represented as an error bar plot in Figure 16, where the mean error and its standard deviation are shown for each operating condition: in black results from knock sensor A and B, and results from the knock sensor C are shown in color grey. Top plots represents results from cylinder 1 and bottom plots results from cylinder 3.

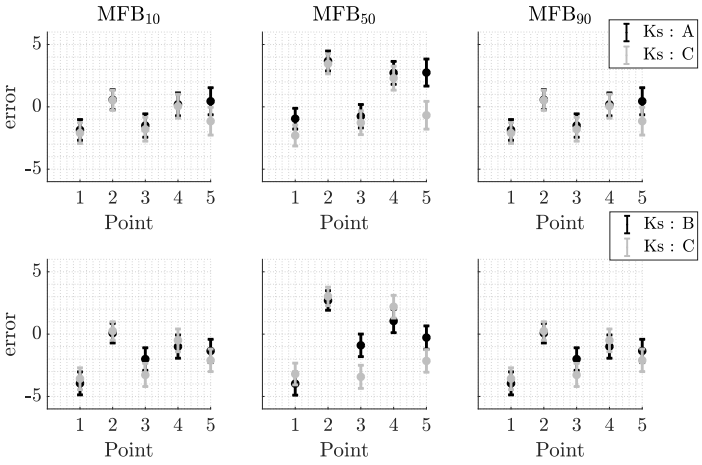

Figure 16: Mean error and standard deviation of CA10 (left), CA50 (middle) and CA90 (right) for all 5 validation points. Cylinder 1 (top) and cylinder 3 (bottom)

As can be seen in Figures 15 and 16, the estimation of the MFBx from the MFB model it is affected by the knock sensor location. Therefore, during next section, a discussion about the impact on the minimum oscillation calculation will be included.

5.2. Minimum oscillation

The objective of modeling the MFB is to be able to determine the evolution of the minimum oscillation required to determine if a cycle is normal or knock combustion, as was shown in Figure 9.

The minimum oscillation required for the end-gas to auto ignite computed from Equation (10) is represented in Figure 17: in black the value is computed by obtaining the MFB from the in-cylinder pressure, in grey line and blue, computing the MFB from the wiebe model when the EOC is obtained from knock sensor A and C respectively.

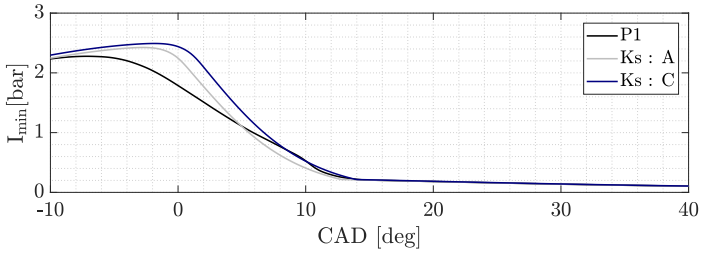

Figure 17: Minimum oscillation required to the end gas to auto ignite estimation according to Equation (10).Operating condition 1.

In order to evaluate the estimation of such evolution, the error between the minimum oscillation computed by the in-cylinder pressure and the knock sensor during a steady test is analyzed in Figure 18. On top plots, cases for

cylinder 1 where left plot is the error when the minimum oscillation is computed from the MFB model considering the EOC from knock sensor A and right plot knock sensor C. On the other hand, bottom plots shows cases for cylinder 3, where left case the EOC is computed from knock sensor B and right plot knock sensor C. In grey all 200 cycles and in black the average error are represented.

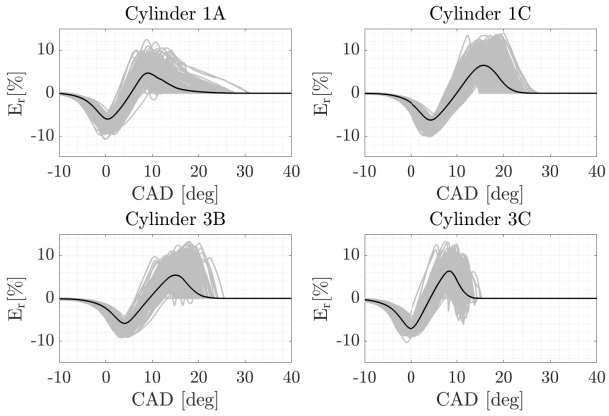

Figure 18: Relative error between in-cylinder pressure and knock sensor signal on the minimum oscillation estimation. Operating condition 1.

As can be seen in Figure 18, even if the MFB model is affected by the knock sensor location as is shown in Figure 16, when computing the minimum oscillation required, $I_{k,min}$, the relative error of the evolution during a cycle is not significantly affected by the knock sensor location, being the error around 10 %. In Figure 19, the I_{min} computed from in-cylinder pressure is represented against the one obtained from knock sensor signal for the operating condition 1, the R^2 is value is also represented for each case.

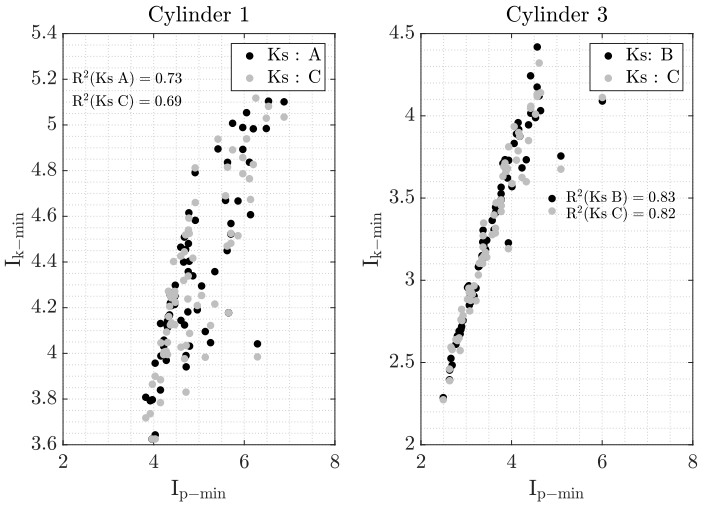

Figure 19: Minimum oscillation (Equation (10)) computed from in-cylinder pressure vs knock sensor. Left plot cylinder 1 and right plot cylinder 3. Operating condition 1.

As can be seen in Figure 19, the R^2 in both cases is higher for the knock sensor closer to the combustion chamber, being for all cases a R^2 value over 0.65. During the following section the knock recognition for both locations will be analyzed in order to evaluate both knock sensor positions for the recognition of the phenomena.

5.3. Knock recognition

The knock recognition method presented in Figure 9 is applied for knock sensors A or B, for cylinders 1 and 3 respectively, and for knock sensor C. Results during this section are compared with the knock recognition when in-cylinder pressure is analyzed as described in [13].

As discussed in section 4, knocking cycles are detected when the maximum of the resonance index is above the minimum oscillation produced by the end gas auto ignition, computed from Equation (10). In Figures 20 and 21 the resonance indexes computed from knock sensors and in-cylinder pressure are analyzed for a normal combustion and a knocking cycle respectively. On the top plots, the resonance index evolution with the threshold are represented, on the left plot for knock sensors signals and on the right plot for in-cylinder pressure. On the bottom plot, the HRR and the band-pass in-cylinder pressure is represented.

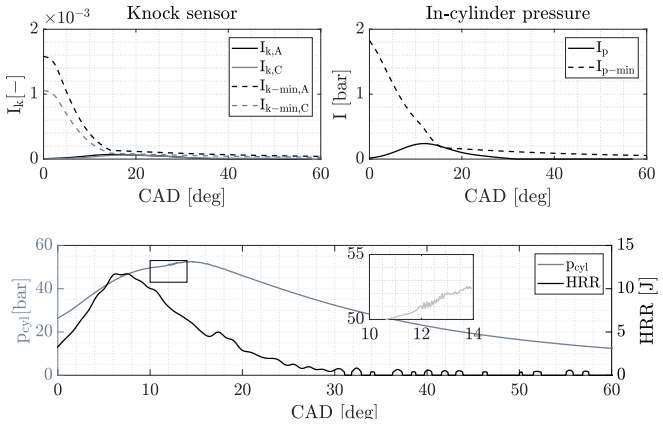

Figure 20: Resonance index evolution and detail cycle (HRR and p_{bp}) for a normal combustion cycle. Operating condition point 3: MAPO 0.27 bar

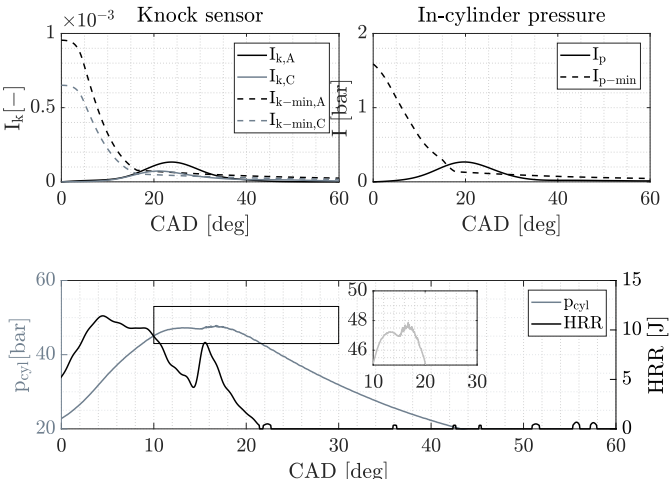

Figure 21: Resonance index evolution and detail cycle (HRR and p_{bp}) for a knocking cycle. Operating condition point 3: : MAPO 0.26 bar.

As it can be seen in Figure 20 and 21, both cycles have a similar MAPO amplitude, but the resonance evolution it is not the same, i.e in normal combustion case the resonance is excited during combustion, near the maximum of the HRR, and on the other hand, for knocking case resonance is rapidly excited at the end of combustion. Notice that zoomed plots have the same y-axis length.

The method was evaluated for in-cylinder pressure and knock sensors signals during different SA settings at steady state conditions. Results are represented in Figure 22, where the knock probability is represented as a function of the SA delay from the calibrated point. The method proposed is compared with two knock recognition methods based on in-cylinder pressure, on the one hand, the MAPO definition with a threshold of 0.4 bar, and on the other hand the high sensitivity method proposed in [13].

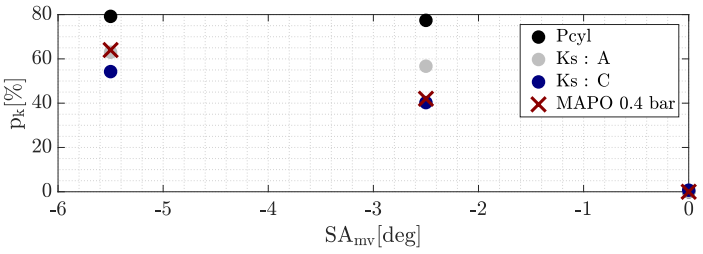

Figure 22: Knock recognition method over a SA sweep point 1 cylinder 1. Operating condition point 3.

For the calibration point, $SA = SA_{mv}$, the knock probability for the three methods is zero, but when advancing the SA knock probability increases for the three sensors. For knock sensor A, the knock probability is closer to the one recognized by the low sensitivity method based on in-cylinder pressure. On the other hand, for knock sensor C, the knock probability also increases when advancing the SA, but the probability is lower. For all SA settings the knock probability from knock sensor A is higher than for MAPO definition, but when delaying the SA until 5.5 from the calibration point, the knock probability from knock sensor C is underestimated.

The method was evaluated over five operating conditions, the knock probability computed for each case is represented in Figure 23, where top plot shows results from cylinder 1 and bottom plot cylinder 3. Different colors are used to highlight results from the different methods.

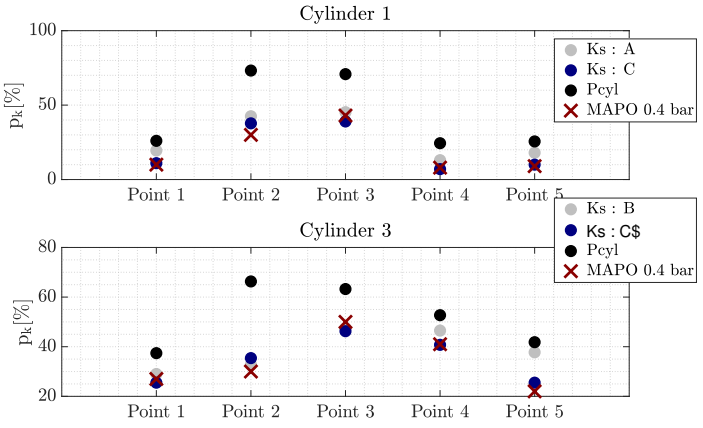

Figure 23: Knock probability computed from the different knock sensor location over five operating conditions.

As can be seen in Figure 23, for all operating conditions the knock probability computed from knock sensor C case is lower than for A and B cases. In all the operating conditions knock probability for knock sensors A and B is lower than the high sensitivity method, but higher than MAPO. On the other hand, for knock sensor C, in operating condition 3 the method proposed with this sensor is

underestimating knock when comparing it with MAPO.

6. Conclusions

In this work a low knock recognition method based on in-cylinder pressure signal was used to develop an alternative method based on knock sensor signal in a spark ignited heavy-duty engine. The method makes use of a Wiebe function and an observer to estimate the knock threshold evolution during a cycle, which is compare with a resonance index computed from knock sensor signal.

The mass fraction burned model based on a Wiebe function is evaluated thought different operating conditions, by comparing the MFBx obtained from the model with the ones computed from in-cylinder pressure measurement. Was demonstrated that for the estimation of the minimum oscillation required for the end gas to auto ignite the Wiebe model leads to a 10 % of relative error, when comparing the minimum oscillation with the one computed from in-cylinder pressure.

Besides, an analysis of the knock recognition sensitivity for two knock sensor locations has been performed over different operating conditions and spark advance settings, demonstrating that the method is able to distinguish knocking events with a high resolution for knock sensors located near the cylinder heads, while less resolution was observed by analyzing one knock sensor located between both cylinders.

The main findings of this work were:

- The low knocking recognition method based on in-cylinder pressure signal developed for light-duty engines is also valid for heavy-duty engines.
- When the method is extended to knock sensor signal, the recognized cycles are less than those obtained with the low knocking recognition method but higher or equal than when applying a fixed threshold, as MAPO.
- For one knock sensor per cylinder configuration the knock recognition resolution is between a high sensitivity method and the classical MAPO limit.
- When the number of knock sensors is halved, the knock recognition resolution is reduced, but a similar knock recognition than when applying a MAPO threshold.

7. Acknowledgments

Irina Jimenez received a funding through the grant GRISOLIAP/2018/132 and BEFPI/2021/042 from the Generalitat Valenciana and the European Social Fund.

References

[1] C. Bae, J. Kim, Alternative fuels for internal combustion engines, Proceedings of the Combustion Institute 36 (3) (2017) 3389–3413.

[2] T. Korakianitis, A. Namasivayam, R. Crookes, Natural-gas fueled spark-ignition (si) and compression-ignition (ci) engine performance and emissions, Progress in energy and combustion science 37 (1) (2011) 89–112.

[3] B. Ashok, K. Nanthagopal, V. Anand, K. Aravind, A. Jeevanantham, S. Balusamy, Effects of n-octanol as a fuel blend with biodiesel on diesel engine characteristics, Fuel 235 (2019) 363–373.

[4] A. C. R. Teixeira, P. G. Machado, F. M. de Almeida Collaco, D. Mouette, Alternative fuel technologies emissions for road heavy-duty trucks: a review, Environmental Science and Pollution Research (2021) 1–16.

[5] H. Wei, R. Zhang, L. Chen, J. Pan, X. Wang, Effects of high ignition energy on lean combustion characteristics of natural gas using an optical engine with a high compression ratio, Energy 223 (2021) 120053.

[6] X. Li, X. Zhen, S. Xu, Y. Wang, D. Liu, Z. Tian, Numerical comparative study on knocking combustion of high compression ratio spark ignition engine fueled with methanol, ethanol and methane based on detailed chemical kinetics, Fuel 306 (2021) 121615.

[7] M. I. Jahirul, H. H. Masjuki, R. Saidur, M. Kalam, M. Jayed, M. Wazed, Comparative engine performance and emission analysis of cng and gasoline in a retrofitted car engine, Applied Thermal Engineering 30 (14-15) (2010) 2219–2226.

[8] S. Sahoo, D. K. Srivastava, Effect of compression ratio on engine knock, performance, combustion and emission characteristics of a bi-fuel cng engine, Energy (2021) 121144.

[9] Z. Chen, Y. Ai, T. Qin, F. Luo, Quantitative evaluation of n-butane concentration on knock severity of a natural gas heavy-duty si engine, Energy 189 (2019) 116244.

[10] A. A. Quader, Lean combustion and the misfire limit in spark ignition engines, SAE transactions (1974) 3274–3296.

[11] C. Park, C. Kim, Y. Choi, S. Won, Y. Moriyoshi, The influences of hydrogen on the performance and emission characteristics of a heavy duty natural gas engine, International journal of hydrogen energy 36 (5) (2011) 3739–3745.

[12] J. B. Heywood, Internal combustion engine fundamentals, McGraw-Hill Education, 2018.

[13] B. Pla, J. De La Morena, P. Bares, I. Jiménez, Knock analysis in the crank angle domain for low-knocking cycles detection, Tech. rep., SAE Technical Paper (2020).

[14] C. S. Draper, Pressure waves accompanying detonation in the internal combustion engine, Journal of the Aeronautical Sciences 5 (6) (1938) 219–226.

[15] X. Zhen, Y. Wang, S. Xu, Y. Zhu, C. Tao, T. Xu, M. Song, The engine knock analysis–an overview, Applied Energy 92 (2012) 628–636.

[16] R. Novella, B. Pla, P. Bares, I. Jiménez, Acoustic characterization of combustion chambers in reciprocating engines: An application for low knocking cycles recognition, International Journal of Engine Research (2020) 1468087420980565.

[17] P. Bares, D. Selmanaj, C. Guardiola, C. Onder, A new knock event definition for knock detection and control optimization, Applied Thermal Engineering 131 (2018) 80–88.

[18] F. Bi, T. Ma, X. Wang, Development of a novel knock characteristic detection method for gasoline engines based on wavelet-denoising and emd decomposition, Mechanical Systems and Signal Processing 117 (2019) 517–536.

[19] D. Siano, M. A. Panza, A nonlinear black-box modeling method for knock detection in spark-ignition engines, in: AIP Conference Proceedings, Vol. 2191, AIP Publishing LLC, 2019, p. 020137.

[20] D. Siano, D. D'agostino, Knock detection in si engines by using the discrete wavelet transform of the engine block vibrational signals, Energy Procedia 81 (2015) 673–688.

[21] B. Pla, J. De La Morena, P. Bares, I. Jiménez, Adaptive in-cylinder pressure model for spark ignition engine control, Fuel 299 (2021) 120870.
[22] G. Brecq, J. Bellettre, M. Tazerout, A new indicator for knock detection in gas si engines, International Journal of Thermal Sciences 42 (5) (2003) 523–532.
[23] X. Shen, Y. Zhang, T. Shen, Cylinder pressure resonant frequency cyclic estimation-based knock intensity metric in combustion engines, Applied Thermal Engineering 158 (2019) 113756.
[24] A. Hoth, C. P. Kolodziej, Effects of knock intensity measurement technique and fuel chemical composition on the research octane number (ron) of face gasolines: Part 1–lambda and knock characterization, Fuel (2021) 120722.
[25] J. Kim, In-cylinder pressure based engine knock classification model for high-compression ratio, automotive spark-ignition engines using various signal decomposition methods, Energies 14 (11) (2021) 3117.
[26] K. Bizon, G. Continillo, S. Lombardi, E. Mancaruso, B. M. Vaglieco, Ann-based virtual sensor for on-line prediction of in-cylinder pressure in a diesel engine, in: Computer Aided Chemical Engineering, Vol. 33, Elsevier, 2014, pp. 763–768.
[27] K. Akimoto, H. Komatsu, A. Kurauchi, Development of pattern recognition knock detection system using short-time fourier transform, IFAC Proceedings Volumes 46 (21) (2013) 366–371.
[28] F. Bi, X. Li, C. Liu, C. Tian, T. Ma, X. Yang, Knock detection based on the optimized variational mode decomposition, Measurement 140 (2019) 1–13.
[29] C. Draper, The physical effects of detonation in a closed cylindrical chamber, Twentieth Annual Report (1935) 361–376.
[30] M. Lapuerta, O. Armas, J. Hernández, Diagnosis of di diesel combustion from in-cylinder pressure signal by estimation of mean thermodynamic properties of the gas, Applied Thermal Engineering 19 (5) (1999) 513–529.
[31] O. Chiavola, G. Chiatti, L. Arnone, S. Manelli, Combustion characterization in diesel engine via block vibration analysis, Tech. rep., SAE Technical Paper (2010).
[32] C. Guardiola, B. Pla, P. Bares, A. Barbier, An analysis of the in-cylinder pressure resonance excitation in internal combustion engines, Applied Energy 228 (2018) 1272–1279.
[33] X. Zhao, Z. Li, Z. Li, L. Wang, Combustion parameters estimation based on multi-channel vibration acceleration signals, Applied Thermal Engineering 158 (2019) 113835.